

Extending the Aerial Image Analysis from the Detection of Tree Crowns

Gabriel da Silva Vieira^{*†1}, Bruno M. Rocha^{*2}, Fabrizzio Soares^{†*3}, Júnio César de Lima^{†4}, Helio Pedrini^{§5}, Ronaldo Costa^{*6}, Júlio Ferreira^{†7}

^{*}Federal University of Goiás, *Pixelab Laboratory*. Goiânia - GO, Brazil.

[†]Department of Computer Science, Southern Oregon University, Ashland - OR, USA

[‡]Federal Institute Goiano, *Computer Vision Laboratory*. Urutaí - GO, Brazil.

[§]Institute of Computing, University of Campinas, Campinas, SP, Brazil.

{¹gabriel.vieira, ⁴junio.lima, ⁷julio.ferreira}@ifgoiano.edu.br, ²rocha3runo@ufg.br, ³soaresf@sou.edu, ⁵helio@ic.unicamp.br, ⁶ronaldocosta@inf.ufg.br

Abstract—In this study, we explore some possibilities of using aerial images captured by Unmanned Aerial Vehicles (UAV) and discuss the benefits of using them in the context of intelligent agriculture. A novel method that supports the detection and segmentation of tree crowns, the delineation of shadows, and which shows the direction of sunlight is presented. It uses simple observation strategies and commonly used digital image processing techniques such as visual color enhancement and perception, morphological operations, and segmentation based on a region growing method. The proposal is evaluated using a dataset with different types of crop areas and pasture lands. The results indicate that the proposal can effectively deal with the detection and segmentation of elements of interest in the scene, as well as the indication of the right side of the light source.

Index Terms—segmentation, unmanned aerial vehicles, tree canopy, tree detection, smart farming, image processing

I. INTRODUCTION

Tree detection is important in many activities, such as silviculture treatment [1], tree growth modeling, species identification and classification [2], plant count study for the management of planting conditions, aid for the assessment of forest damage [3], and construction of 3D models of trees [4]. Information on these activities is important, for example, for the modeling of different economic attributes, such as the volume of wood and the supply of bioenergy [5].

One way to perform the mapping of trees in a given region is to traverse the entire region through the soil, performing tree inspection and counting manually. However, this type of mapping presents some challenges besides being very expensive. In rural areas, due to the complexity of the ecosystem, there are places of difficult access, which do not have roads, making it impossible for vehicles to enter [6]. In addition, these regions contain obstacles such as cliffs, waterfalls, rivers, and gorges [7].

An alternative to minimize these challenges is the use of unmanned aerial vehicles (UAV) to capture aerial images for the tree mapping. The UAV is an aircraft that does not have a human pilot on board, and it is controlled remotely employing a communication and operation system [8]. The use of UAV has the following advantages: flexibility of flight time and route, cost reduction, ease of handling, data with high

accuracy, and it does not offer immediate risk to the human being [9]. The UAV can be used for different activities, for example, the collected data can be used to provide tree analysis through the estimation of variables as position, height, and diameter of tree crowns [10], as well as in the identification of plant species and their health for smart farming [6].

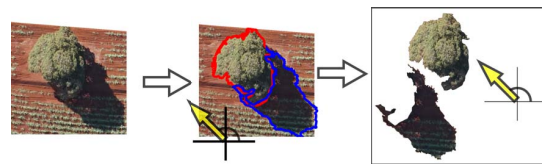


Fig. 1: Main components of the proposed method: tree crown detection and segmentation, shadow delineation, and identification of the light source.

Despite the benefits offered by the use of UAV, it is still challenging to obtain relevant ecological information from the acquired images. For this reason, the analysis of the captured data is often based on visual interpretation, which can achieve significant results. However, the other hand, it can be very laborious and hard to do for large areas [6]. Because of that, efficient and effective algorithms are being implemented for tree segmentation, as in the detection of trees from aerial images [11], [12]. Thus, if these solutions provide satisfactory results, they can be used to estimate, for instance, the productivity of crop areas.

Figure 1 illustrates the main components that constitute the proposed approach. Initially, an aerial image is processed, then the crown of a tree and its own shadow are detected and segmented. After that, trees and shadows are used to show the direction of the light source. This study extends the aerial image analysis by investigating uses of it and by presenting a method that employs digital image processing techniques in the context of object detection and recognition in rural areas.

In this paper, we present a novel method that supports three main requirements: (i) the detection and segmentation of tree crowns that are in crop and pasture fields; (ii) the delineation of tree shadows; and (iii) the indication of the light source

direction.

This text is organized as follows. Section II describes relevant works that are related to this research. Section III presents our proposal to segment tree crowns, to delineate tree shadows, and to indicate the direction of the source light. Section IV presents some results and a discussion about the performance of our method. Finally, the conclusions and future work are exposed in Section V.

II. RELATED WORK

Klein et al. [12] produced a new toolbox for tree segmentation. This toolbox used several scripts already implemented in ArcGIS¹ for its full operation. The watershed segmentation algorithm was in the core of the TreeDetect segmentation process. A UAV was used to capture images of young and adult Eucalyptus and Pinus from tree plantations, and also from a natural mixed hardwood forest. TreeDetect proved to be efficient for segmentation of trees in the different captured images.

Similarly, Huang et al. [11] used aerial images captured by UAV for tree segmentation. Their work aimed to perform tree segmentation by applying bias field estimation to reduce the within-canopy spectral heterogeneity in aerial images. Some forest nursery images were segmented by the marker-controlled watershed algorithm. To evaluate the method, a visual interpretation between the manual (each tree crown was manually drawn) results and the developed technique was made. In addition, the F-score index was used to assess accuracy.

Yang et al. [2] developed a method for delineating tree crowns in broadleaf tree species. The multispectral watershed segmentation was applied to individual tree crown delineation, and they have manually digitized the position of the reference crowns. The crowns had visually different in textures, shapes, and sizes. This variety of visual characteristics was used to evaluate the transferability and robustness of the proposed method.

III. PROPOSED METHOD

The proposed method is divided into three components that deal with (i) tree crown detection and segmentation, (ii) shadow delineation, and (iii) identification of the light source (direction of the sun). The first two components work independently, but the last one depends on the first two components. This section introduces each of these components, their modeling design, and the influence of choosing their parameters in recognition of the required objects. Besides, the parameterization of the proposed method is evaluated using statistical measures.

The true positive rate (TPR, Eq. 1) and false positive rate (FPR, Eq. 2) are used as statistical measures to analyze the influence of parameterization on the results. While the TPR shows the correct hit percentage in the correct class, the FPR shows the proportion of class that was erroneously recognized.

¹<https://www.arcgis.com>.

The objective is to find some ideal arguments that maximize the TPR values while minimizing the FPR value. In this section, as well as in Section IV, the same image dataset is used in which the classes are labeled as follows:

- True Positive (TP): pixels that are correctly identified in the positive class (tree crown or shadow area).
- True Negative (TN): pixels that are correctly identified as not belonging to a positive class.
- False Positive (FP): pixels that are incorrectly identified in the positive class.
- False Negative (FN): pixels that are not designated as belonging to a positive class when, in fact, they are.

$$\text{TPR} = \frac{\text{TP}}{\text{TP} + \text{FN}} \quad (1) \quad \text{FPR} = \frac{\text{FP}}{\text{FP} + \text{TN}} \quad (2)$$

A. Tree Crown Detection

Let \mathbf{I}_{RGB} be an input RGB image of size $m \times n$, where the three channels are $r_{i,j} \in \mathbf{R}$, $g_{i,j} \in \mathbf{G}$, and $b_{i,j} \in \mathbf{B}$, for $i \in \{1, \dots, n\}$ and $j \in \{1, \dots, m\}$. We start by exceeding the green color channel. Firstly, the relationship between the three channels is evaluated according to Eq. 3.

$$\begin{aligned} \forall i, j \quad \ddot{a}_{i,j} &= [(r_{i,j} - g_{i,j}) > 0] \wedge [(r_{i,j} - g_{i,j}) < v] \\ \forall i, j \quad \ddot{b}_{i,j} &= g_{i,j} > (\bar{g} - \sigma_G) \\ \forall i, j \quad \ddot{c}_{i,j} &= g_{i,j} < (\bar{g} + \sigma_G) \end{aligned} \quad (3)$$

where v is a term that requires a small value (as $v = 10$, in a value range from 0 to 255). \bar{g} and σ_G are the mean and standard deviation of the \mathbf{G} channel, respectively.

Then, the \mathbf{G} channel is updated. Eq. 4 shows how it is performed.

$$\begin{aligned} \forall i, j \quad e_{i,j} &= (\ddot{a}_{i,j} \wedge \ddot{b}_{i,j} \wedge \ddot{c}_{i,j}) \\ \forall i, j \quad g'_{i,j} &= \begin{cases} g_{i,j} + (r_{i,j} - g_{i,j}), & \text{if } e_{i,j} = \text{true} \\ g_{i,j}, & \text{otherwise} \end{cases} \end{aligned} \quad (4)$$

where the logical values $\ddot{a}_{i,j}$, $\ddot{b}_{i,j}$, and $\ddot{c}_{i,j}$ are used to create \mathbf{E} . $e_{i,j} \in \mathbf{E}$ is a logical value, from image \mathbf{E} , that maps the green pixels. It is used to update only the supposed green pixels in channel \mathbf{G} .

The non-green pixels are then removed based on Eq. 5, in which $x_{i,j} \in \mathbf{X}$ holds the maximum values among the pixels in the RGB image channels. $c_{i,j}^{(g)} \in \mathbf{C}_g$ is a binary image which contains only the supposed green pixels.

$$\begin{aligned} \forall i, j \quad x_{i,j} &= \max(r_{i,j}, g'_{i,j}, b_{i,j}), \\ \forall i, j \quad c_{i,j}^{(g)} &= \begin{cases} 1, & \text{if } g'_{i,j} = x_{i,j} \\ 0, & \text{otherwise} \end{cases} \end{aligned} \quad (5)$$

Two morphological operations are applied on \mathbf{C}_g : a closing operation followed by an opening operation with a circular structured element with radius τ . Then, each connected component $w \in W$ of this image receives an identification k , such that its size and circularity are evaluated. Components that have fewer pixels than a threshold α are discarded. In Eq. 6, the perimeter P and the area A of a connected component w_k , for $k \in \{1, \dots, \lambda\}$, is stored in the vector $Y = (y_1, y_2, \dots, y_\lambda)$ in

the position k , and λ is the number of connected components in the image \mathbf{C}_g .

$$\forall k \quad y_k = \frac{P^2(w_k)}{4\pi A(w_k)} \quad (6)$$

Values y_k in the vector Y that are smaller than a threshold γ are used to discard their corresponding elements from \mathbf{C}_g . Finally, the radii of the remaining elements are computed and used to draw circles on the image, to extract the tree crown areas and to obtain the final result \mathbf{I}_{tc} , which is an image with only the trees.

Table I shows an evaluation of the parameterization of the proposed method. Clearly, some of the best arguments for parameters τ , α , and γ are 3, 10 and 2×10^3 , respectively.

args	τ		γ		α (args $\times 10^3$)	
	TPR	FPR	TPR	FPR	TPR	FPR
1	0.50	0.02	0.00	0.00	0.88	0.08
2	0.79	0.03	0.14	0.00	0.85	0.05
3	0.84	0.05	0.44	0.01	0.84	0.05
4	0.84	0.06	0.44	0.01	0.82	0.05
5	0.78	0.11	0.56	0.01	0.80	0.04
6	0.80	0.16	0.79	0.02	0.76	0.03
7	0.78	0.19	0.79	0.02	0.76	0.03
8	0.81	0.19	0.83	0.05	0.74	0.03
9	0.49	0.09	0.85	0.07	0.71	0.03
10	0.48	0.10	0.85	0.05	0.71	0.03

TABLE I: Parameter evaluation: tree crown segmentation.

B. Shadow Delineation

To delineate the shadows, we consider a hypothesis in which the lower intensities of aerial images of cropland and pasture fields correspond to shades of trees. Firstly, a median filtering operation with a $\kappa \times \kappa$ kernel is applied on the input RGB image \mathbf{I}_{RGB} , generating a resulting image $\mathbf{I}_{Med} = (\mathbf{R}_{Med}, \mathbf{G}_{Med}, \mathbf{B}_{Med})$. Then, Eq. 7 is used to identify points that are in darker areas. It is a simple function that receives an image channel and calculates the minimum value of this channel.

$$m^{(z)} = \min_{\mathbf{I}_c \in \{\mathbf{R}_{Med}, \mathbf{G}_{Med}, \mathbf{B}_{Med}\}} (\mathbf{I}_c) \quad (7)$$

where \mathbf{I}_c is a channel R, G, or B of the image \mathbf{I}_{Med} , and $M' = (m^{(1)}, \dots, m^{(h)})$ stores the minimum value of these channels, for $z \in \{1, \dots, h\}$, where $h = 3$ is the number of channels. As Eq. 7 returns only one value for each image channel, we have made it more flexible by using a β term. Then, pixels values of $a'_{i,j} \in \mathbf{I}_c$, which are smaller than $m^{(z)} + \beta$, are selected according to Eq. 8.

$$\forall i, j, z \quad m^{(z)}_{i,j} = \begin{cases} a'_{i,j}, & \text{if } a'_{i,j} \leq m^{(z)} + \beta \\ -1, & \text{otherwise} \end{cases} \quad (8)$$

Values of $m^{(z)}_{i,j}$ are used in the next step in a region growing algorithm, which is a way to separate the image into simple regions with homogeneous behavior. The region-based segmentation requires two arguments: a seed point and a tolerance value. In our method, the seed points are the values

of $m^{(z)}_{i,j} > -1$ named as s , whereas the tolerance is defined by the term δ . In Eq. 9, the intensities of the pixels from the filtered image \mathbf{I}_c (i.e. R, G, and B channels) are evaluated to yield h binary images \mathbf{B}' .

$$s = m^{(z)}_{i,j} \\ \forall i, j, z \quad b^{(z)}_{i,j} = \begin{cases} 1, & \text{if } (s > -1) \wedge (|a'_{i,j} - s| \leq \delta) \\ 0, & \text{otherwise} \end{cases} \quad (9)$$

Finally, following Eq. 10, the binary images $\mathbf{B}' = \{\mathbf{B}^{(1)}, \dots, \mathbf{B}^{(h)}\}$, where $b^{(z)}_{i,j} \in \mathbf{B}^{(z)}$, are used to delineate the shadows of the trees and to yield a final image \mathbf{I}_{sw} that contains only the shadows.

$$\mathbf{I}_{sw} = \mathbf{B}^{(1)} \vee \mathbf{B}^{(2)} \vee \mathbf{B}^{(3)} \quad (10)$$

We also evaluated the shadow delineation parameters in which some of the best arguments for κ , β , and δ were 15, 10 and 10, respectively.

C. Light Source Direction

In the last two sections, the segmentation of tree crowns and shadows were presented independently of one other. That means we could not tell which shadow belonged to which tree. In this section, we define an association rule to identify the relationship between shadows and trees. The definition is based on the assumption that there is an overlap between the corresponding elements. Thus, if there is an intersection between them, their relationship is perceived.

The elements of \mathbf{I}_{tc} and \mathbf{I}_{sw} are labeled to map the intersection between tree crowns and shadows. In Eq. 11, the intersection between these two images are used to this purpose.

$$\mathbf{I}_{it} = \mathbf{I}_{tc} \cap \mathbf{I}_{sw} \quad (11)$$

To deal with multiple shadows that are intersected with the same segment of a tree crown, we consider two constraints: (i) a shadow can not be fully inserted into a tree crown segment; and (ii) the shadow that has the largest area of intersection is chosen. Finally, we calculate the center of mass of each corresponding element and, based on their centroids, we draw a line between these two points whose origin is in the delineated shadow. The direction of this line points toward the direction of the light source.

IV. RESULTS AND DISCUSSION

To evaluate our method, we prepared a database with aerial images, acquired by a UAV, organized into three types of environments that differ from one another by ground composition (vegetation type and terrain). The study areas are located at Goiânia and Quirinópolis, Goiás, Brazil, and their locations are (16°36'S, 49°15'W - 29 ha) and (18°36'S, 50°25'W - 24 ha), respectively. This database contains trees that are within typical crop areas, pasture fields, and within clean lands (i.e., without crops and bushes, but with trees). These images are in RGB format and were downsampled to 601×601 pixels.

This section is divided into two subsections. The first one presents a quantitative evaluation based on statistical measures,

where the second presents a qualitative analysis through visual inspections, respectively.

A. Quantified Results

In addition to TPR and FPR metrics, we considered in this section the positive and negative predictive values (PPV and NPV, Eq(s). 12 and 13), the bookmaker informedness (BM, Eq. 14, where $TNR = 1 - FPR$), and F_1 score (Eq. 15).

$$PPV = \frac{TP}{TP+FP} \quad (12) \quad NPV = \frac{TN}{TN+FN} \quad (13)$$

$$BM = TPR + TNR - 1 \quad (14) \quad F_1 = 2 \cdot \frac{PPV(TPR)}{PPV + TPR} \quad (15)$$

Table II presents the results for the tree crowns segmentation and also for the shadows delineation. These rates range from 0 to 1, where larger values are preferred, except for the FPR measure. Positive classes were well detected, as shown by TPR and PPV rates and, according to NPV, the negative classes were also well detected. In addition, FPR showed that few mistakes were made, and BM and F_1 showed that the assertiveness of the proposed method is high, more significant than 70%.

	TPR	FPR	PPV	NPV	BM	F_1
Crowns	0.86	0.05	0.59	0.98	0.81	0.70
Shadows	0.72	0.03	0.69	0.97	0.69	0.71

TABLE II: Statistical masures.

The errors were also investigated considering other metrics in order to verify the bias and dispersion of the data concerning the reference images. Thus, the mean bias error (MBE), mean square error (MSE), normalized cross-correlation (NCC), and an estimate of the area under the ROC curve through the $A_{d'}$ function were used. In addition, we considered the Structural Similarity Index (SSIM) [13] for measuring image quality. In Eq(s) 16, 17 and 18, $\mathbf{U} \in \{\mathbf{I}_{sw}, \mathbf{I}_{tc}\}$ corresponds to an image index, and \mathbf{U}^t is the ground-truth image, where $u_{i,j} \in \mathbf{U}$ and $u_{i,j}^t \in \mathbf{U}^t$. In Eq. 19, the ϕ function converts ω scores into probabilities and the ϕ^{-1} converts probabilities into ω scores, where $d' = \phi^{-1}(TPR) - \phi^{-1}(FPR)$ (details are shown in [14]).

$$MBE = \frac{1}{nm} \sum_{i=1}^n \sum_{j=1}^m \frac{u_{i,j} - u_{i,j}^t}{u_{i,j}^t} \quad (16)$$

$$MSE = \frac{1}{nm} \sum_{i=1}^n \sum_{j=1}^m \left(\frac{u_{i,j} - u_{i,j}^t}{u_{i,j}^t} \right)^2 \quad (17)$$

$$NCC = \frac{1}{nm} \sum_{i=1}^n \sum_{j=1}^m \frac{u_{i,j} u_{i,j}^t}{(u_{i,j}^t)^2} \quad (18)$$

$$A_{d'} = \phi \frac{d'}{\sqrt{2}} \quad (19)$$

Table III presents the errors between the outputs from the proposed method concerning the reference images from the used dataset. Because the MBE measures the systematic error caused by the incorrect estimation of the two classes, it showed that the residual errors in our tests were considerably

small, close to 0. The total errors presented by MSE also are approximately 0, demonstrating how well the quality of our approach is in terms of correct class recognition. Furthermore, $A_{d'}$ shows that the assertiveness of our method was high, whereas NCC and SSIM values showed that the structures of the images were entirely preserved.

	Error Measures					Detection evaluation	
	MBE	MSE	$A_{d'}$	NCC	SSIM	SR	FR
Crowns	0.04	0.05	0.97	0.87	0.84	75.5%	8.16%
Shadows	0.01	0.03	0.96	0.76	0.84	80.0%	8.88%

TABLE III: Error measures and detection of tree crowns and shadows with success rate (SR) and failure rate (FR).

Table III also shows the results when evaluating the proposed method for detection of tree crowns and shadows. The success rate (SR) is computed based on the correct identification of the positive class (crowns or shadows), and the failure rate (FR) is referred to the percentage of wrong segments that were labeled as a positive class.

B. Visual Inspection

Visual results of the detection and segmentation process are presented in Figure 2, where two original images are presented. Non-green pixels are discarded, and the shape of each remaining connected component is analyzed to preserve only quasi-circular shapes. Then, the radius of each connected component is used to detect and segment the tree crowns. Only a few errors can be noticed, mainly due to non-tree areas, which are similar to tree crowns, and due to the exclusion step of small connected components that erroneously removed small tree crowns.

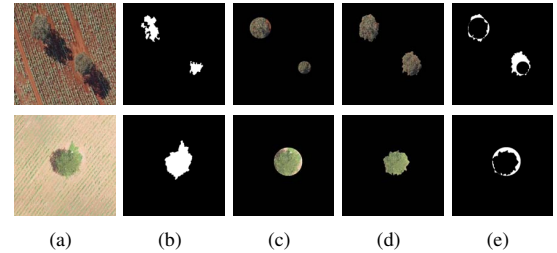


Fig. 2: Detection and segmentation of tree crowns. (a) original images; (b) quasi-circular elements; (c) segmented crowns; (d) ground truth; (e) difference between (c) and (d).

Figure 3 presents some results from the shadow delineation process. A median filter is applied and the minimum values of the intensities of the pixels are used as seed points to a region growing algorithm. Then, the tree shadows are detected and segmented from the original images. Ground truth images are used to evaluate the quality of the shadow delineation method, and the differences between the detected shadows and the ground truth present the areas that were wrongly labeled. We can note that the segmentation exceeds the shadow areas and parts of the tree crowns are labeled as shadows.

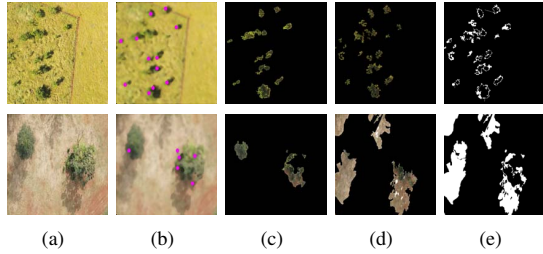


Fig. 3: Shadow delineation. (a) original images; (b) filtered image and seed points; (c) segmented shadows; (d) ground truth; (e) difference between (c) and (d).

In Figure 4, the light source direction is detected and appointed. As the tree crowns and shadows were preliminary detected, an association rule between them shows the right side of the light source. This rule is based on the intersection between crowns and shadows in which the center of mass of the correlated connected components are used to point a line that originates in the shadow areas and ends in the tree crowns.

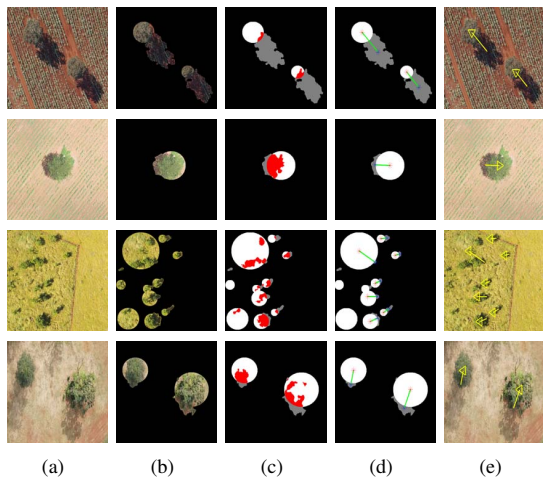


Fig. 4: Sunlight direction. (a) original images; (b) segmented tree crowns and shadows; (c) intersection between crowns and shadows; (d) center of mass of these elements; (e) source light direction.

V. CONCLUSIONS AND FUTURE WORK

In this paper, we applied some digital image processing techniques to detect and segment tree crowns, to delineate shadow areas, and to indicate the origin of the light source. The proposed method was divided into three components, each one responsible for supporting the detection of trees, shadows, and direction of the sunlight. The proposed method was evaluated using a dataset with different types of crop areas and pasture lands, and the results demonstrated that the detection and segmentation were well performed, as well as the indication of the right side of the light source.

Although this work has yielded substantial results, some limitations of the proposed method can be pointed out such as its use in dense forests, where tree crowns are closely connected. We intend to address such limitations in a further investigation. In addition, we plan to work with aerial temporal images in order to track areas covered by tree shadows and also to map the influence of the sunlight on those covered areas. Thus, the detection of regions with lower light incidence and the indication of regions that require natural shadows might contribute to the planned planting of crops and trees.

ACKNOWLEDGMENTS

The authors would like to thank CNPq and CAPES for their financial support.

REFERENCES

- [1] W. Wan Mohd Jaafar, I. Woodhouse, C. Silva, H. Omar, K. Abdul Maulud, A. Hudak, C. Klauberg, A. Cardil, and M. Mohan, "Improving Individual Tree Crown Delineation and Attributes Estimation of Tropical Forests Using Airborne LiDAR Data," *Forests*, vol. 9, no. 12, p. 759, Dec. 2018.
- [2] J. Yang, Y. He, J. P. Caspersen, and T. A. Jones, "Delineating Individual Tree Crowns in an Uneven-Aged, Mixed Broadleaf Forest Using Multi-spectral Watershed Segmentation and Multiscale Fitting," *IEEE Journal of Selected Topics in Applied Earth Observations and Remote Sensing*, vol. 10, no. 4, pp. 1390–1401, Apr. 2017.
- [3] M. Mohan, C. Silva, C. Klauberg, P. Jat, G. Catts, A. Cardil, A. Hudak, and M. Dia, "Individual Tree Detection from Unmanned Aerial Vehicle (UAV) Derived Canopy Height Model in an Open Canopy Mixed Conifer Forest," *Forests*, vol. 8, no. 9, p. 340, Sep. 2017.
- [4] J. Jiao and Z. Deng, "Individual Building Rooftop and Tree Crown Segmentation from High-Resolution Urban Aerial Optical Images," *Journal of Sensors*, vol. 2016, pp. 1–13, 2016.
- [5] J. Yang, Y. He, J. P. Caspersen, and T. A. Jones, "Delineating Individual Tree Crowns in an Uneven-Aged, Mixed Broadleaf Forest Using Multi-spectral Watershed Segmentation and Multiscale Fitting," *IEEE Journal of Selected Topics in Applied Earth Observations and Remote Sensing*, vol. 10, no. 4, pp. 1390–1401, Apr. 2017.
- [6] S. Baena, J. Moat, O. Whaley, and D. S. Boyd, "Identifying species from the air: UAVs and the very high resolution challenge for plant conservation," *Plos One*, vol. 12, no. 11, Nov. 2017.
- [7] C. B. Anderson, "The CCB-ID approach to tree species mapping with airborne imaging spectroscopy," *PeerJ*, vol. 6, Oct. 2018.
- [8] ICAO, *Unmanned aircraft systems: UAS*, ser. ICAO circular. Montréal: International Civil Aviation Organization, 2011, no. 328, oCLC: 729908130.
- [9] X. Wu, X. Shen, L. Cao, G. Wang, and F. Cao, "Assessment of Individual Tree Detection and Canopy Cover Estimation using Unmanned Aerial Vehicle based Light Detection and Ranging (UAV-LiDAR) Data in Planted Forests," *Remote Sensing*, vol. 11, no. 8, p. 908, Apr. 2019.
- [10] J. Guerra-Hernandez, E. Gonzalez-Ferreiro, A. Sarmento, J. Silva, A. Nunes, A. C. Correia, L. Fontes, M. Tomé, and R. Diaz-Varela, "Short Communication. Using high resolution UAV imagery to estimate tree variables in Pinus pinea plantation in Portugal," *Forest Systems*, vol. 25, no. 2, p. eSC09, Jul. 2016.
- [11] H. Huang, X. Li, and C. Chen, "Individual Tree Crown Detection and Delineation From Very-High-Resolution UAV Images Based on Bias Field and Marker-Controlled Watershed Segmentation Algorithms," *IEEE Journal of Selected Topics in Applied Earth Observations and Remote Sensing*, vol. 11, no. 7, pp. 2253–2262, Jul. 2018.
- [12] A. M. Klein Hentz, A. P. D. Corte, S. Péllico Netto, M. P. Strager, and E. R. Schoeninger, "Treedetection: Automatic Tree Detection using UAV-based Data," *Floresta*, vol. 48, no. 3, p. 393, Jun. 2018.
- [13] Z. Wang, A. C. Bovik, H. R. Sheikh, E. P. Simoncelli *et al.*, "Image quality assessment: from error visibility to structural similarity," *IEEE Transactions on Image Processing*, vol. 13, no. 4, pp. 600–612, 2004.
- [14] H. Stanislaw and N. Todorov, "Calculation of signal detection theory measures," *Behavior Research Methods, Instruments, & Computers*, vol. 31, no. 1, pp. 137–149, 1999.